IOPscience iopscience.iop.org

Home Search Collections Journals About Contact us My IOPscience

Effects of the image potential on hydrogenic impurity binding energies in quantum well wires

This article has been downloaded from IOPscience. Please scroll down to see the full text article.

1993 J. Phys.: Condens. Matter 5 2261

(http://iopscience.iop.org/0953-8984/5/14/021)

View the table of contents for this issue, or go to the journal homepage for more

Download details:
IP Address: 171.66.16.159
The article was downloaded on 12/05/2010 at 13:10

Please note that terms and conditions apply.

J. Phys.: Condens. Matter 5 (1993) 2261–2266. Printed in the UK

Effects of the image potential on hydrogenic impurity binding energies in quantum well wires

Zhen-Yan Deng† and Shi-Wei Gu†‡

†Department of Applied Physics and Institute of Condensed Matter Physics, Shanghai Jiao Tong University, Shanghai 200030, People's Republic of China

‡Chinese Centre of Advanced Science and Technology (World Laboratory), PO Box 8730, Beijing 100080, People's Republic of China

Received 20 October 1992

Abstract. The effects of the image potential on hydrogenic impurity binding energies in quasi-one-dimensional GaAs/AlAs quantum well wires with a rectangular cross section are investigated. The results have shown that, when the impurity ion image potential is considered, the variations in binding energy are considerable and, when the impurity ion and electron image potentials are considered simultaneously, the corresponding variations in binding energy are small. The results also showed that the image potential is important, especially when the cross section dimensions of the quantum wire become small.

1. Introduction

With the recent advances in molecular beam epitaxy techniques, it is now possible to grow wire-like compound semiconductor structures of low nanometre size. Because of the quantum confinement in two directions, the binding energies of excitions and impurity states are greatly enhanced in the wires compared with those in quasi-two-dimensional quantum well structures. Much theoretical interest has been devoted to the study of hydrogenic impurity states in these quasi-one-dimensional semiconductor systems [1–4]. However, in these studies the image potentials of impurity ions and electrons due to the dielectric mismatch inside and outside the quantum well wire are neglected. Recently several researchers have considered the image potential in semiconductor interfaces and heterostructures and found that the results are interesting and the image potential is important [5–9]. Gabovich and Rozenbaum [5] have studied the potential energy of the image forces in MIS structures, and their results agree with experimental data on electron tunnelling in MIS structures. Lee and Antoniewicz [6, 7] have investigated the electron bound states and surface polaron in the vicinity of two orthogonal surfaces, including the electron image potential. Cappellini and Delsole [8] have calculated the effects of image potential perturbation on the direct and inverse angle-resolved normal photoemission at an Si–GaAs semiconductor interface, and the results have shown that the energy shifts due to image potential are of the order of tens of millielectronvolts. In addition, in [10] the impurity ion image potential is included in the calculation of the impurity binding energies in quantum well structures, but the amount of change in binding energy due to the image potential is left unknown.

0953-8984/93/142261+06$07.50 © 1993 IOP Publishing Ltd

The question is whether or not the effects of the image potential on the impurity binding energies are negligible. In this paper we discuss this problem by introducing impurity ion and electron image potentials in quasi-one-dimensional GaAs/AlAs quantum well wires. In our calculation, the effective-mass approximation and variational approach are adopted. Also, we considered only the ground electronic states whose energies (less than 200 meV) are much smaller than the conduction band offset (1.07 eV) between AlAs and GaAs; so the potential barrier between AlAs and GaAs is assumed to be infinitely high.

The paper is organized as follows. In section 2 we explain the Hamiltonian of hydrogenic impurity states including the image potential. The numerical results and discussion are presented in section 3.

2. Hamiltonian

Let us consider a quantum wire of GaAs surrounded by AlAs, which is assumed to have a rectangular cross section and an infinitely high potential barrier between GaAs and AlAs. In the effective-mass approximation, the Hamiltonian describing the motion of an electron in the quantum wire can be written

$$H^{(0)}(\boldsymbol{r}) = |\boldsymbol{p}|^2/2m^* + V_0 \tag{1}$$

where $\boldsymbol{p}$ and $\boldsymbol{r}$ are the electron momentum and coordinate, respectively, and m^* is the electron-band effective mass which is $m^* = 0.067m_0$ in GaAs with m_0 the free-electron mass. The electron-confining potential well V_0 is given by

$$V_0 = \begin{cases} 0 & |x| < d_x, |y| < d_y \\ \infty & \text{elsewhere} \end{cases} \tag{2}$$

where $2d_x$ and $2d_y$ are the widths of the rectangular quantum wire.

The energy levels of the unperturbed quantum well wire are given by

$$E_{mnk_z} = E_{mn} + \hbar^2 k_z^2/2m^* \tag{3a}$$

$$E_{mn} = (\hbar^2\pi^2/8m^*)(m^2/d_x^2 + n^2/d_y^2) \tag{3b}$$

corresponding to the envelope functions

$$\psi_{mnk_z}(\boldsymbol{r}) = \phi_{mn}(x, y)(1/L^{1/2})\exp(ik_z z) \tag{4a}$$

$$\phi_{mn}(x, y) = [1/(d_x d_y)^{1/2}]\sin[(m\pi/2d_x)\ (x + d_x)]\sin[(n\pi/2d_y)\ (y + d_y)] \tag{4b}$$

where $m, n = 1, 2, \ldots$, and L is the length of the quantum wire.

When a hydrogenic impurity is placed in the quantum wire, the Hamiltonian is

$$H^{(1)}(\boldsymbol{r}) = |\boldsymbol{p}|^2/2m^* - e^2/\epsilon_1[(x - x_0)^2 + (y - y_0)^2 + z^2]^{1/2} + V_0 \tag{5}$$

where $\epsilon_1 = 13.1$ is the static dielectric constant of GaAs and $(x_0, y_0, 0)$ is the position of the hydrogenic impurity in the quantum wire.

Now we let the dielectric mismatch between GaAs and AlAs be expressed as

$$p = (\epsilon_1 - \epsilon_2)/(\epsilon_1 + \epsilon_2) \tag{6a}$$

$$p' = (\epsilon_{1\infty} - \epsilon_{2\infty})/(\epsilon_{1\infty} + \epsilon_{2\infty}) \tag{6b}$$

with $\epsilon_2 = 10.1$ the static dielectric constant of AlAs, and $\epsilon_{1\infty} = 10.9$ and $\epsilon_{2\infty} = 8.16$ the optical dielectric constants for GaAs and AlAs respectively. The positions of the ion image charges are obtained as follows:

$$\begin{aligned} x_0^+(l) &= 2[\![\{l - [(l+1)/2]\}(d_x + x_0) + [(l+1)/2](d_x - x_0)]\!] + x_0 \\ x_0^-(l) &= -2[\![[(l+1)/2](d_x + x_0) + \{l - [(l+1)/2]\}(d_x - x_0)]\!] + x_0 \\ y_0^+(k) &= 2\,[\![\{k - [(k+1)/2]\}(d_y + y_0) + [(k+1)/2](d_y - y_0)]\!] + y_0 \\ y_0^-(k) &= -2\,[\![[(k+1)/2](d_y + y_0) + \{k - [(k+1)/2]\}(d_y - y_0)]\!] + y_0 \end{aligned} \tag{7}$$

where $k, l = 0, 1, 2, \ldots$, and $[x] = \text{int}\ x$. The electronic Hamiltonian including the impurity ion image potential can be written as

$$H^{(2)}(r) = |p|^2/2m^* + V_1(r) + V_0 \tag{8}$$

where

$$V_1(r) = -\frac{e^2}{\epsilon_1} \sum_{l,k=0}^{\infty} \sum_{i,j} p^{l+k} \{[x - x_0^i(l)]^2 + [y - y_0^j(k)]^2 + z^2\}^{-1/2} \tag{9}$$

is the sum of the impurity ion and its image potentials, where $i, j = +, -$.

In the practical variational calculation, a finite number of image charges were included in the expansion of equation (9). Since the dielectric mismatch p is about 15%, the contribution due to high-order image charge terms could be neglected. In our calculation, we have tried to include the image charges up to first- and second-order terms, respectively, and found that the differences between the binding energies of the two cases are below 4%. So we consider the impurity ion image potential only up to second-order terms.

According to the analysis above, when we further consider the electron image potential, only the interaction between the electron and its first four image charges are included in order to simplify our calculation, i.e.

$$H^{(3)}(r) = |p|^2/2m^* + V_1(r) + V_2(r) + V_0 \tag{10}$$

where

$$V_2(r) = C_1/(d_x^2 - x^2) + C_2/(d_y^2 - y^2) \tag{11}$$

is the electron image potential and

$$C_1 = (1/\epsilon_{1\infty})p' \tfrac{1}{2} d_x e^2 \qquad C_2 = (1/\epsilon_{1\infty})p' \tfrac{1}{2} d_y e^2. \tag{12}$$

Because the image potentials of impurity ions and electrons are small compared with the impurity ion potential, the trial wavefunction of $H^{(j)}(r)$ $(j = 1, 2, 3)$ that we take is analogous to that used in [1–4] and is written for the ground impurity state as

$$\psi(r) = N \cos[(\pi/2d_x)x'] \cos[(\pi/2d_y)y'] \exp\{-[(x - x_0)^2 + (y - y_0)^2 + z^2]^{1/2}/\lambda\} \tag{13}$$

where N is the normalization constant and λ is the variational parameter. The trial wavefunction (13) satisfies the boundary conditions.

As usual, we define the impurity binding energy as the energy difference between the bottom of the electronic conduction band without the impurity and the ground level of the impurity state in the quantum wire, i.e.

$$E_i^{(j)} = (\hbar^2\pi^2/8m^*)(1/d_x^2 + 1/d_y^2) - \min_{\lambda} \langle \psi(r) | H^{(j)}(r) | \psi(r) \rangle \tag{14}$$

where $j = 1, 2, 3$. The above integrals were calculated numerically.

3. Results and discussion

According to the geometric symmetry of the quantum wire, we consider only the impurity binding energies in one rectangular cross section and the following typical points and lines are selected. In figure 1, O, A, and B are the centre, the centre of one side and the corner of the cross section, respectively, the lines OA, OB, and AB connecting these three points.

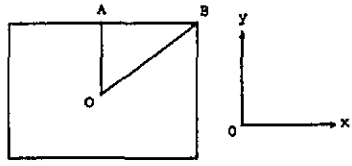

Figure 1. The rectangular cross section of the quantum wire. O, A and B are the centre, the centre of one side and the corner of the quantum wire, respectively.

Figure 2 shows the variations in the impurity binding energy with its position on different lines in the cross section of the quantum wire, where we set the cross section sizes $d_x = d_y = 50$ Å. In figure 2 the full curves represent the impurity binding energies without the image potential, and the broken curves and chain curves represent the impurity binding energies including the impurity ion image potential and including the impurity ion and electron image potentials, respectively.

From figure 2, it is apparent that, when the impurity ion image potential is added, the impurity binding energies change markedly. The differences $E_i^{(2)} - E_i^{(1)}$ between the binding energies in the two cases including and without the impurity ion image potential at points O, A and B are 6.50 meV, 5.73 meV and 5.47 meV, respectively. When the impurity moves towards one side or the corner of cross section, these differences decrease subsequently. In figure 2, we also found other interesting results as follows. When the impurity ion and electron image potentials are added simultaneously, the corresponding variations in impurity binding energy are small compared with those considering only the impurity ion image potential. The differences $E_i^{(3)} - E_i^{(1)}$ between the binding energies of the cases including and without the impurity ion and electron image potentials at points O, A and B are 1.44 meV, 0.91 meV and 0.58 meV, respectively. Also, when the impurity moves towards the boundary of cross section, the variations in binding energy tend to decrease.

Figure 3 shows the variations in impurity binding energy with the cross section dimensions $d_x = d_y$ of quantum wire at three typical points O, A and B. As in figure 2, here the full curves also represent the impurity binding energies without the image potential, and the broken curves and chain curves represent the impurity binding energies including the impurity ion potential and including the impurity ion and electron image potentials, respectively. In figure 3, it can be easily seen that the differences between the impurity binding energies of the cases including and without the image potential at the three points O, A and B increase with decrease in cross section dimensions. When the cross section sizes $d_x = d_y = 250$ Å, the differences $E_i^{(2)} - E_i^{(1)}$ between the impurity binding energies of the two cases including and without the impurity ion image potential at the three points O, A and B are 2.16 meV, 1.58 meV and 1.34 meV, respectively, and the differences $E_i^{(3)} - E_i^{(1)}$ between the impurity binding energies of the cases including and without the impurity ion and electron image potentials at points O, A and B are 0.55 meV,

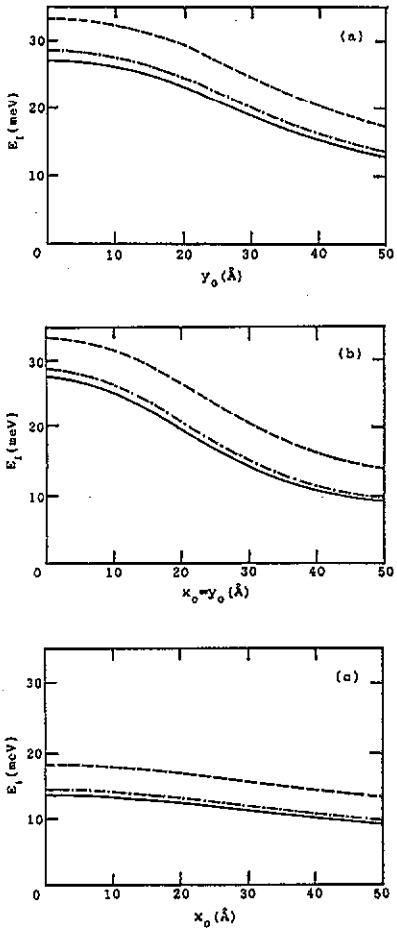

Figure 2. Numerical results for impurity binding energies on (*a*) line OA, (*b*) line OB and (*c*) line AB in the cross section of the quantum wire, where the cross section sizes $d_x = d_y = 50$ Å. The full curves represent the impurity binding energies without considering the image potential, and the broken curves and chain curves represent the corresponding impurity binding energies including the impurity ion image potential and including the impurity ion and electron image potentials, respectively.

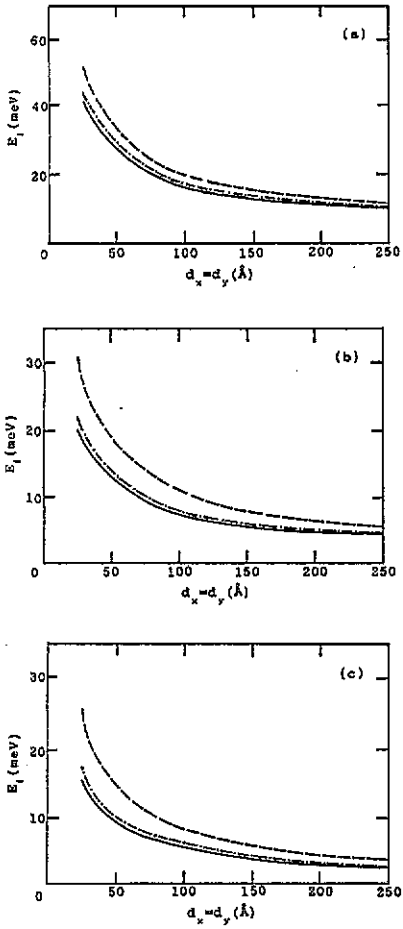

Figure 3. The variations in impurity binding energy with cross section dimensions $d_x = d_y$ at the three points (*a*) O, (*b*) A and (*c*) B in the quantum wire. The full curves represent the impurity binding energies without considering the image potential, and the broken curves and chain curves represent the corresponding impurity binding energies including the impurity ion image potential and including the impurity ion and electron image potentials, respectively.

0.48 meV and 0.40 meV, respectively. When the cross section sizes are reduced to $d_x = d_y = 25$ Å, the corresponding differences $E_i^{(2)} - E_i^{(1)}$ at the three points O, A and B are 11.83 meV, 10.78 meV and 9.65 meV, respectively, and the corresponding differences $E_i^{(3)} - E_i^{(1)}$ at the points O, A and B are 2.16 meV, 1.70 meV and 1.30 meV, respectively.

The results obtained above are interesting and their physical interpretation and discussion are as follows. From equations (6), we can see that the dielectric mismatches p and p' between GaAs and AlAs are larger than zero; so the impurity

ion image potential in equation (9) is negative. This is the reason for the marked increase in impurity binding energies when the electronic Hamiltonian included the impurity ion image potential. In contrast, from equation (11), we can also see that the electron image potential is positive, and the impurity ion and electron image potentials cancel each other. As a result, when the sum of the impurity ion and electron image potentials is added, the variations in impurity binding energy become small. In addition, when the cross section sizes decrease, the quantum confinement of electrons is strengthened, and the interaction potential between the electrons and image charges increases. This results in an increase in the differences between the impurity binding energies of the cases including and without the image potential. The results obtained above remind us that the image potential in the quantum wire is important. Strictly speaking, the image potential in the quantum wire cannot be neglected in calculating the impurity binding energies, especially when the cross section dimensions of the quantum wire become small. When the impurity binding energies in the quantum wire are calculated, both the impurity ion and the electron image potentials should be included in the electronic Hamiltonian simultaneously and not only the impurity ion image potential considered.

In conclusion, we have studied the effects of the image potential on hydrogenic impurity binding energies and found that, when only the impurity ion image potential is included, the variations in binding energy are considerable and, when the impurity ion and electron image potentials are considered simultaneously, the variations in impurity binding energy become small. The results also showed that the differences between the binding energies of the cases including and without the image potential increase with decrease in the cross section dimensions of the quantum wire. These remind us that the image potential should be considered in calculating the impurity binding energy, especially when the cross section dimensions of the quantum wire are small.

Acknowledgment

This work was supported by the National Committee of Education and National Science Foundation of China grant 69188006.

References

[1] Brum J A 1985 *Solid State Commun.* **54** 179
[2] Bryant G W 1985 *Phys. Rev.* B **31** 7812
[3] Weber G, Schulz P A and Oliveira L E 1988 *Phys. Rev.* B **38** 2179
[4] Osorio F A P, Degani M H and Hipolito O 1988 *Phys. Rev.* B **37** 1402
[5] Gabovich A M and Rozenbaum V M 1985 *Sov. Phys.–Solid State* **27** 468
[6] Lee W W and Antoniewicz P R 1989 *Phys. Rev.* B **40** 3352
[7] Lee W W and Antoniewicz P R 1989 *Phys. Rev.* B **40** 9920
[8] Cappellini G and Delsole R 1991 *Solid State Commun.* **79** 185
[9] Pokutnyi S I and Efremov N A 1991 *Phys. Status Solidi* b **165** 109
[10] Mailhiot C, Chang Y C and McGill T C 1982 *Phys. Rev.* B **26** 4449